RESEARCH PAPER

PCCP
www.rsc.org/pccp

Level of theory study of magnetic resonance parameters of chalcogen XY^- (X, Y = O, S and Se) defects in alkali halides†

F. Stevens,[ab] V. Van Speybroeck,[a] E. Pauwels,[a] H. Vrielinck,[b] F. Callens[b] and M. Waroquier*[a]

[a] *Laboratory of Theoretical Physics, Ghent University, Proeftuinstraat 86, B-9000 Ghent, Belgium. E-mail: michel.waroquier@UGent.be; Fax: +32 9 264 65 60*

[b] *Department of Solid State Sciences, Ghent University, Krijgslaan 281-S1, B-9000 Ghent, Belgium*

Received 12th August 2004, Accepted 18th November 2004
First published as an Advance Article on the web 9th December 2004

An extensive level of theory study is performed on diatomic chalcogen defects in alkali halide lattices by density functional theory methods. A variety of exchange correlation functionals and basis sets are used for the calculation of electron paramagnetic resonance (EPR) parameters of XY^- (X, Y = O, S, Se) molecular ions doped in MZ (M = Na, K, Rb and Z = Cl, Br, I) lattices. Various factors contribute to the EPR values, such as geometrical effects, the choice of basis set and functional form. A sensitivity analysis is made by comparing experimental and theoretical magnetic resonance data. A flow scheme is proposed for obtaining the best agreement between experimental and calculated *g*-values for chalcogen defects in alkali halides.

1. Introduction

Diatomic XY^- defects (X, Y = O, S, Se) in chalcogen doped alkali halide lattices are presently studied in solid state physics because they exhibit an extremely intense superfluorescence behavior under laser excitations at low temperatures.[1–4] Such materials have a potential for use in new high-gain mirrorless lasers. Additionally, these ions are also studied in the context of biological applications. Indeed, the superoxide ion is the primary reactive oxygen species ubiquitously produced in biological respiration and metabolism.[5,6]

Consequently, diatomic chalcogen defects in alkali halides have been intensively studied using electron paramagnetic resonance (EPR) and optical techniques since the late 1950s. Pioneering EPR work has been done by Känzig *et al*. and Zeller *et al*.[7–9] on the superoxide molecular ion. In the following years, this EPR work was extended toward the S_2^-, Se_2^- and SSe^- ions by Morton and Vannotti *et al*.[10–13] In the 1980s and 1990s, new crystal growth methods were applied to facilitate the incorporation of these defects in other alkali halides than those investigated by Morton and Vannotti and these defects were further investigated using electron nuclear double resonance (ENDOR) techniques.[14–25] For nearly all defects studied, a model was proposed in which the XY^- molecular ion replaces a single halide ion, *i.e*. a single-vacancy model. Recently, the validity of this model was confirmed by density functional (DFT) calculations for S_2^-, SSe^- and Se_2^- defects.[26,27] Using density functional methods, EPR parameters of transition metal ions doped in alkali halide lattices are presently studied.[29–34]

Due to the wealth of experimental EPR data available for XY^- defects in alkali halides, these systems are ideally suited for testing various theoretical calculation methods. The objective of this paper is to perform an extensive level of theory study using density functional techniques on the theoretical simulation of *g*-tensors of XY^- defects in alkali halides. Various factors contribute to the final result of the magnetic resonance data: geometry, cluster size, choice of basis set and exchange correlation functional. The various computational schemes are validated by convergence of the resulting spin Hamiltonian parameters and by comparison with the experimental data. The final goal is to present a computational flow scheme for accurate simulation of *g*-tensors for chalcogen defects in alkali halide lattices.

The paper is organized as follows. In Section 2, a short discussion of the spin Hamiltonian parameters used in the analysis of the XY^- molecular ions is given. The computational details are summarized in Section 3. Section 4 gives a thorough discussion of the various model ingredients having a substantial influence on the calculated g data. Additionally, computed hyperfine values are compared with the available experimental ones. A suitable computational protocol for calculating *g*-values of chalcogen defects in MZ lattices (M = Na, K, Rb and Z = Cl, Br, I) is presented. The main conclusions are given in Section 5.

2. Theory of EPR parameters

In this section, we discuss briefly some tensorial spin Hamiltonian parameters which can be deduced from EPR experiments. For the theoretical principles of EPR, we refer to literature (see *e.g*. see in ref. 35). We only summarize the most relevant expressions. The spin Hamiltonian used for the interpretation of EPR spectra of systems with one unpaired electron (effective spin $S = 1/2$) is given by

$$\hat{H} = \beta_e \hat{\vec{S}} \bar{g} \vec{B} + \sum_i \hat{\vec{S}} \bar{A}_i \hat{\vec{I}}_i \qquad (1)$$

with $\mu_B = e\hbar/2m_e$ the Bohr magneton (m_e is the electron mass).

The first term in this equation is the electronic Zeeman term, which describes the interaction between the electron spin $\vec{S}$ and the external magnetic field $\vec{B}$ and is parameterized by the *g* tensor.

The second term represents the interaction between the electron spin $\vec{S}$ and a nuclear spin $\vec{I}_i$ involving the hyperfine

† Electronic supplementary information (ESI) available: Calculated *g*-values, relaxations and hyperfine couplings as functions of increasing basis size. See http://www.rsc.org/suppdata/cp/b4/b412408a/

DOI: 10.1039/b412408a

tensor $\bar{\boldsymbol{A}}_i$. This tensor is often decomposed into an isotropic and an anisotropic part. The isotropic part is related to the probability of finding the electron at the nucleus. The anisotropic part of the hyperfine tensor is due to the interaction between magnetic dipoles and yields additional information about the wavefunction and the local environment of the unpaired electron.

The free X_2^- and XY^- molecular ions have a $D_{\infty h}$ and $C_{\infty v}$ symmetry and a $(n\pi_g)^3$ and $(n\pi)^3$ (n = 2,3,4) electron configuration, respectively. In the alkali halide crystal lattice, the symmetry is lowered to D_{2h} and C_{2v}. The degeneracy of the π_g and π orbitals is lifted and either a $^2B_{2g}$ (Fig. 1a) or a $^2B_{3g}$ (Fig. 1b) ground state results for the X_2^- molecular ions. In Fig. 1, the spin density for the RbCl : S_2^- ($^2B_{2g}$ ground state, Fig. 1a) and NaCl : S_2^- ($^2B_{3g}$ ground state, Fig. 1b) defect structures are shown. For the XY^- molecular ions, the corresponding possibilities are $^2B_1$ and $^2B_2$. The observed symmetry is orthorhombic-I ($g_x \neq g_y \neq g_z \neq g_x$) and the principal axes are oriented along [110] (g_z), [$\bar{1}$10] (g_x) and [001] (g_y) or equivalent conformations, (Fig. 1). According to the theory of Känzig *et al.*[7–9] and Maes *et al.*,[21] the g tensor is characterized by $g_x < g_y < g_z$ if the molecular ion has the $^2B_{2g}$ or $^2B_1$ ground state and by $g_x < g_y < g_z$ in case of the $^2B_{3g}$ or $^2B_2$ ground state. The smallest g value is found along the direction of the paramagnetic p lobes of the molecular ion.

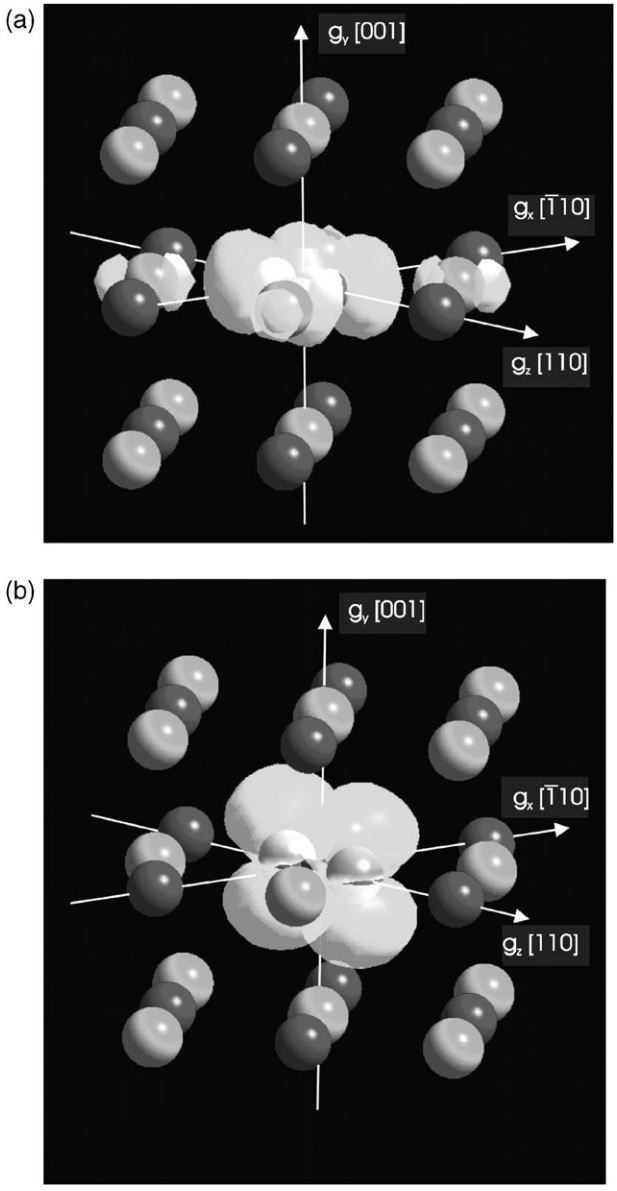

Fig. 1 Spin density distribution for the RbCl : S_2^- ($^2B_{2g}$ ground state), (a) and the NaCl : S_2^- ($^2B_{3g}$ ground state), (b) defect structures. In both cases, the same spin-density cut off was used.

3. Computational details

3.1. Details of calculation

The Amsterdam Density Functional (ADF) program package, version 1999[36–38] was used to optimize the geometries of each of the studied MZ : XY^- defect structures. When calculations are performed with the ADF program package, four exchange correlation functionals are used, belonging to the local density approximation (LDA) and general gradient approximation (GGA): VWN,[39] Bp86,[40,41] BLYP[41–44] and Pw91[45] with basis sets I (single-ζ, SZ), II (double-ζ, DZ), III (double-ζ with polarization function, DZP), IV (triple-ζ with polarization function, TZP) and V (triple-ζ with two polarization functions, TZ2P). A frozen core approximation was applied for all atoms (Na.2p, K.3p, Rb.4p, Cl.2p, Br.3d and I.4d) except for the central molecular ion and the first shell alkali atoms.[27] In this notation, Na.2p means that the frozen core approximation is applied up to the 2p electron shell. Theoretical *g*- and hyperfine values were obtained by the methods developed by Van Lenthe *et al.*[46,47] The relativistic atomic potentials or effective core potentials, which are used during the EPR calculations, were calculated using the auxiliary program DIRAC,[48] which is supplied with the ADF program package. For the calculation of *g*-values, a spin–orbit (SO) restricted open shell (ROKS) approach has been used, while for the calculation of hyperfine couplings a scalar relativistic (SR) unrestricted (UKS) approach, as both implemented in ADF, has been used.

Calculation of g and hyperfine tensors were also performed with the Gaussian 2003 (G03) program package[49] as G03 provides a much wider choice of exchange and correlation functionals and basis sets than ADF. All calculations using G03 were performed at a spin unrestricted level of theory. It should be stressed that all G03 applications in this work for the evaluation of the EPR parameters are based on geometrical structures which were determined using ADF. The authors believe that a comparative analysis of the results obtained with these two programs should be incorporated in a thorough study concerning the level of theory. Seven different density functionals were used in the G03 calculations: VWN,[39] Bp86,[40,41] B3LYP,[42,50] B3Pw91,[45,51,52] B3P86,[42,50] PBE1PBE[53] and BHandHLYP.[54] The following basis sets were used:[55,56] EPR-II,[57] 6-31G**,[58,59] 6-311G**,[60–62] augg-cc-pV6Z[63–65] and Sadlej.[66–69]

In the following we use a compact but transparent notation indicating unambiguously the level of theory used in the geometry optimization and that employed for the evaluation of the EPR parameters, *e.g.*: the notation VWN/IV//B3LYP/6-311G**/6-31G** means that the geometry optimization was performed at the VWN/IV level while the subsequent EPR calculations were performed using a B3LYP exchange correlation functional with a basis set 6-311G** for the defect and 6-31G** for the neighboring lattice shells.

3.2. Implementation of *g*-values

For completeness, we briefly point out the main differences between the implementation of the *g*-tensor in the ADF and G03 packages. Detailed descriptions can be found in ref. 46 (ADF) and ref. 70 (G03).

The ADF package uses basis sets of Slater-type orbitals and is restricted to non-hybrid density functionals. In the absence of an external magnetic field, orbitals are determined by a spin-restricted open shell DFT calculation (no spin polarization). Spin–orbit (SO) coupling is included in the DFT Hamiltonian H_0, using the zero order regular approximation (ZORA,[71–74]), $H_0 = V + \vec{\sigma} \cdot \vec{p}(K/2)\vec{\sigma} \cdot \vec{p}$, where $K = 2c^2/2c^2 - V$. In the SCF potential V, the usual non-relativistic approximations for the

exchange–correlation potential are made. SO effects are treated to all orders and the response to a small external magnetic field can be calculated with simple first-order perturbation theory.

For an open-shell Kramers doublet molecule, the *g*-tensor in this approach is determined by the matrix elements $\langle \Phi_i | H^Z | \Phi_j \rangle$ of the Zeeman interaction,

$$H^Z = \frac{g_e}{2c}\left[\frac{K}{2}\vec{\sigma}\cdot\vec{B}^0 + \frac{K}{4}\vec{B}^0\cdot\vec{L} + \vec{B}^0\cdot\vec{L}\frac{K}{4} + \vec{\sigma}\cdot\left(\vec{\nabla}\frac{K}{2}\times\vec{A}^0\right)\right], \quad (2)$$

taken between both members $\Phi_{1,2}$ of the degenerate doublet. Ref. 46 presents further details about how gauge-invariance is restored when using a finite basis set, employing the method of gauge-including atomic orbitals (GIAOs), and how the scaled ZORA energy expression is included in the evaluation of the g-values.

The G03 package uses a Gaussian-type basis set, and the implemented method allows for the use of hybrid density functionals and a spin-unrestricted structure calculation. Both SO coupling and the external magnetic field are treated perturbatively. Starting from spin-unrestricted unperturbed SCF results (without SO and magnetic field), the first-order corrections to the spin–orbitals in the presence of a magnetic field are determined with coupled-perturbed SCF theory. This requires the solution of a linear system of large dimensionality (except when non-hybrid functionals are used). The *g*-tensor shift then follows from the knowledge of the first-order spin–orbitals and the matrix elements of the SO interaction between the zeroth order occupied and empty orbitals. Restoration of gauge invariance was implemented by using GIAO orbitals.

Note that two-electron contributions to the SO interaction are not explicitly considered; in G03 the effective one-electron approximation is used,

$$H_{\mathrm{SO}} = \sum_{A,i}\frac{\alpha^2 Z_A^{\mathrm{eff}}}{2|\vec{r}_i - \vec{R}_A|^2}\vec{l}_A(i)\cdot\vec{s}(i) \quad (3)$$

where the Z_A^{eff} are empirical effective nuclear charges.[70] In the method of the ADF package, part of the two-electron contributions (spin-same-orbit) are effectively taken into account by the Kohn–Sham potential in the SO operator; this does not hold for the spin-other-orbit contibutions.

4. Flow scheme for EPR calculations

In this section a computational scheme is developed for the evaluation of *g*-tensors of paramagnetic defects in chalcogen doped alkali halides. The various factors contributing to the final g tensor are systematically investigated. Additionally, theoretical hyperfine values are compared with the available experimental ones. Due to the limited number of experimental hyperfine data available, no final statement concerning these data can be made. Prior to these calculations, an overview of the available simulation methods is given.

4.1. Simulation schemes for modeling defects embedded in a lattice environment

Defects in an ionic lattice environment can be modeled by various computational methods. The most widely used schemes are: (i) a cluster *in vacuo* approximation, (ii) an embedded cluster model and (iii) periodic calculations.

(i) In the first model scheme, the calculations are performed on a cluster which is simply a part of the bulk. Conceptually, this approximation is based on the fact that the local atomic environment in the interior of a sufficiently large cluster forms a good approximation of that of the bulk. By effectively treating only the region of the solid in the immediate vicinity of the defect, this approach can be used to investigate the EPR properties of the defect and the neighboring lattice ions in a direct way. This cluster *in vacuo* method has been used in the simulation of organic radicals,[75] metals,[76] semiconductors[77] and ionic systems.[78] This scheme has proven to give accurate EPR data for the induced defects in chalcogen doped alkali halide lattices,[26,27,79] and will be retained in this work.

(ii) In the second model scheme, the model space consist of a small cluster which is embedded into the potential produced by the rest of the bulk. The latter approach is referred as embedded cluster calculations (ECC). In this scheme, the Evjen point charge procedure is used to simulate the long-range Coulomb interactions.[80] The short-range lattice interactions are taken into account by total-ion potentials.[81,82] The total charge of cluster, total ion potential and point charges must be neutral. The latter method has been applied to the study of transition metal complexes in alkali halide lattices[28–34] and alkali metal doping of MgO surfaces.[83]

(iii) The last, and probably the most natural, way to simulate the lattice is by performing periodic calculations. In this approach the radical is properly embedded in the crystalline environment and boundary effects are eliminated by imposing periodic boundary conditions. It is, however, important to enlarge the unit cell artificially to prevent that defects in neighboring lattice cells are too close to each other. The molecular orbitals are expanded in a plane wave basis set.

In Table I of the electronic supplementary information (ESI),† experimental *g*-values for various defect structures are compared with computed data using the cluster *in vacuo* model and the embedded cluster approach. Calculations using the cluster *in vacuo* model are performed using the computational flow scheme as developed below, while for the embedded calculations a somewhat different approach is applied as described in ref. 29. For these calculations, a cluster with 28 atoms was cut out of the optimized 88 atom cluster (see below) and properly embedded. For all calculations, the ADF program package is applied and basis set IV was used. As is clear from the results reported in Table I of the ESI,† large similarities are noticed in the computed *g*-values of both methods. For the KI : O_2^- defect structure, predictions based on the embedded cluster approach are in somewhat less agreement with experimental data as compared to the cluster *in vacuo* results. Also, in a recent work of the authors, periodic calculations[84,85] have been performed for the KCl : O_3^- defect structure by use of the Car–Parrinello molecular dynamics (CPMD) code.[86] Large similarities were found between the geometries obtained from the cluster *in vacuo* approach and the periodic calculations. In view of the similar results as predicted by the three model, and in view of the most satisfactory reproduction of the *g*-tensor values by the cluster *in vacuo* model, we give preference to the latter model which is systematically applied in the following.

4.2. Determination of the cluster size and number of relaxed lattice shells

Cluster size. To find the optimum cluster *in vacuo* model for chalcogen defects in alkali halide lattices, some geometrical and electrostatic considerations need to be made. Indeed, as only a small part of the complete lattice is considered, it is expected that the best results will be obtained using a cluster for which the total charge is minimal and for which the electrostatic Madelung potential at the halide vacancy is well reproduced. As shown in ref. 26, a cluster composed of 88 atoms fulfils the above requirements for the simulation of XY^- ions in a single-vacancy configuration.

In order to better justify the final choice of the cluster size, additional calculations using the ADF program package, have been performed for the S_2^- defect in NaCl with emphasis on the convergence behavior of the *g*-factor, charge and Madelung constant. The results of these calculations are shown in Fig. 2a. The 28 atom cluster is composed of the first three

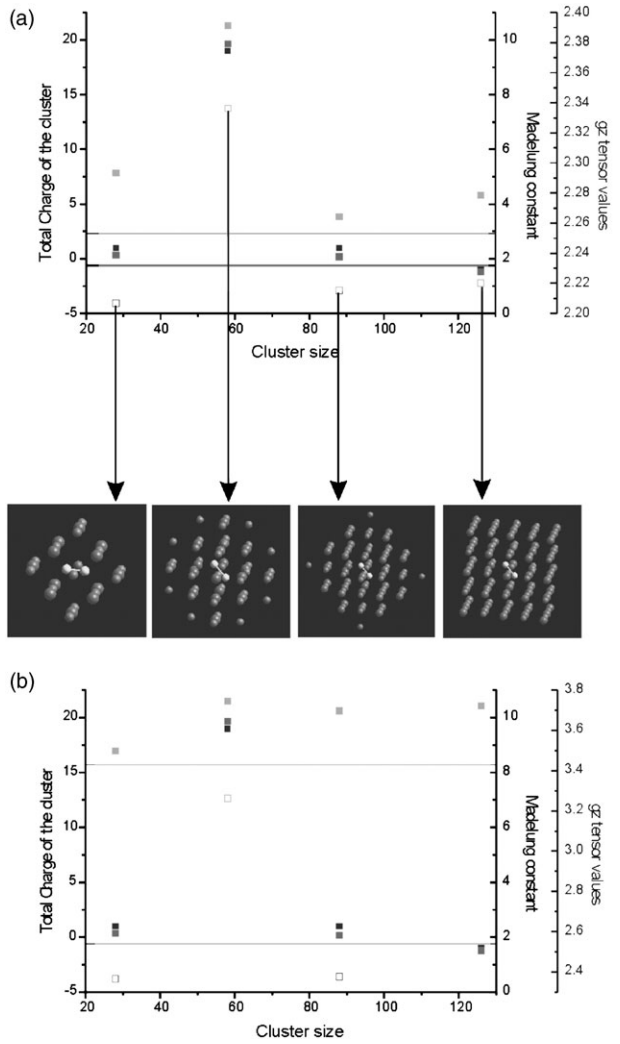

Fig. 2 Total charge, Madelung constant and g_z value in terms of the cluster size (28, 58, 88 and 126) for the NaCl: S_2^- (2(a)) and KCl: S_2^- (2(b)) defect structure. Full squares correspond with the ADF/VWN/IV level while open squares correspond with the G03/B3LYP level. In all G03 calculations a 6-31G** basis set was used for the lattice environment, while a 6-311G** basis set was used for the central defect.

lattice shells, has a charge of +1 and a Madelung constant of 2.133. The 58 atom cluster has a charge of +19 and a Madelung constant of 9.86. Also, the g_z value shows a bump at this cluster size. This emphasis the importance of the total charge and the electrostatic potential at the S_2^- site. The two next clusters consist of 88 and 126 atoms, respectively. The charge varies from +1 to −1 and the Madelung constant oscillates about the value of 1.7475 [87] for the infinite NaCl lattice (2.068 for the 88 atom cluster while 1.516 for the 126 atom cluster). All these data, which were obtained using the ADF program package, are shown in the figure and are valid for the VWN functional. All geometry optimizations were performed at the VWN/IV level of theory within ADF (for more details we refer to the next subsection). About the 28 atom cluster it is important to note that the geometry was optimized in an 88 atom cluster, relaxing the central molecular ion and the first two neighboring lattice shells (see below). The smaller cluster was then cut out from the larger one, keeping the geometry fixed. The g_z value is not yet converged completely for the 126 atom cluster, but, as will be stated below, the cluster size effects are negligible compared with the effects generated by the choice of the functional. In Fig. 2b the same analysis is made for the S_2^- defect in KCl lattice. No noticeable differences are observed between the 88 and 126 atom cluster. This study justifies the choice of an 88 atom cluster to be suitable in ADF calculations for treating defects inside alkali halides and gives an excellent compromise between computation time and numerical accuracy. The same exercise is done for the hybrid B3LYP functional implemented in G03. Due to the immense computational cost to optimize an 88 atom cluster in G03 with hybrid functionals and large basis sets, we prefer to perform all geometry optimizations at the VWN/IV level of theory within ADF. The optimized structures are then used as input in G03 for the evaluation of the wavefunctions and corresponding *g*- and hyperfine values. This method is very suitable to estimate the effects of the applied functional on the EPR parameters. The results are shown in Table II of the ESI.† The geometries of both 28 and 88 atoms clusters are the same. The predicted *g*-values generated by the 28 atom and 88 atom clusters are very close to each other. It seems justified to reduce the cluster size to 28 atom for EPR calculations in G03 in view of the computational cost of enlarging the cluster size. Table I of the ESI† also shows that the hybrid B3LYP functional has a tendency to deviate more from experiment than those obtained with other functionals. In some lattices the disagreement from the experiment is very large. In particular we mention the case of the S_2^- defect in KCl as given in Fig. 2b. The B3LYP estimates (open squares) are far from experiment. To overrule the argument that these large deviancies are possibly due to the lack of convergence, we studied the cluster size effects on the computed B3LYP g_z values by extending the cluster to 126 atoms (displayed by open squares in Fig. 2a). Although a slight improvement is noticed between experiment and theoretical prediction, the differences between the theoretical *g*-values using the 28, 88 and 126 atom clusters are small with respect to the changes induced by varying the functional form. The extension to an 126 atom cluster for the description of the NaCl : S_2^- defect structure was computationally very extensive and we have not repeated this calculation for the KCl lattice as we could expect a similar result. Fig. 2b confirms that the B3LYP predictions for the *g*-tensor obtained in an 28 atom cluster are somewhat similar to those obtained in an 88 atom cluster. They confirm what was expected: the hybrid functional is not able to predict correct g_z-values and this poor reproduction is not due to cluster size effects. The underlying physical reason for this "good behavior" of the 28 atoms cluster is that the total charge is kept low and that the Madelung value at the halide vacancy is well reproduced. For more details we refer to ref. 87.

Relaxation of neighboring lattice shells. The defects under study have a different size compared to the halide ion they replace and thus it seems necessary to take relaxations of neighboring lattice shells into account. To determine the number of lattice shells that need to be relaxed during the optimization, the convergence behavior of the theoretical *g*-values as a function of the number of relaxed lattice shells is studied for NaCl : S_2^- using various functional forms. The results are schematically shown in Fig. 3. A similar investigation was performed for the NaCl : O_2^- defect structure and the same conclusions as for S_2^- can be made. These results are shown in Fig. 1 of the ESI.† Geometry optimizations were performed at the VWN/IV level of theory. It will be validated in section 4.3. that this optimization scheme gives sufficient accuracy. For all functional forms, convergence is reached if the central molecular ion, the first alkali and halide lattice shells are allowed to relax. Further relaxing the lattice environment induces no significant changes (or improvements) of the theoretical *g*-values. In the rest of the paper we will systematically use the 88 atom cluster for geometry optimization in which the central XY^- ion and the first two lattice shells, *i.e.*, the first alkali and the first halide shell, are allowed to relax.

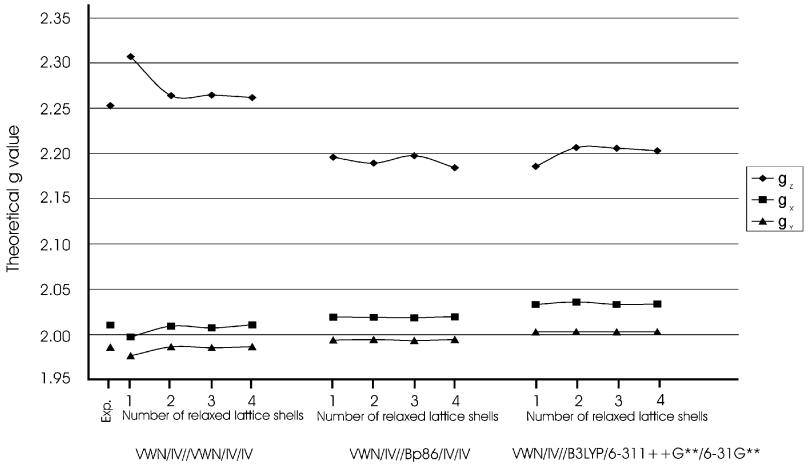

Fig. 3 Calculated *g*-values for NaCl : S_2^- using the VWN/IV//VWN/IV/IV (ADF), VWN/IV//Bp86/IV/IV/ (ADF) and VWN/IV//B3LYP/6-311G**/6-31G** (G03) functional form as a function of the number of neighboring lattice shells that are allowed to relax. The lattice shells that are allowed to relax are labeled 1 to 4: 1 for the six nearest alkali ions, 2 for the twelve next-nearest halide ions, 3 for the eight next-next-nearest alkali atoms and 4 for the six halide ions located on a (200) position.

4.3. Geometry optimization scheme

Convergence in terms of basis sets. In Fig. 4, some characteristic features of the optimized geometry (using ADF) are shown in terms of increasing basis set (I to V) for various exchange correlation functionals (VWN, Bp86, BLYP and Pw91). Fig. 4a displays the internuclear distance of the diatomic defect while all other figures relate to the relaxations of the lattice ions. The latter are all referred to the undisturbed lattice positions. A similar investigation was performed for the NaCl : O_2^- and NaCl : Se_2^- defect structures and the same conclusions as for S_2^- can be made. These results are included in Figs. 2 and 3 of the ESI.

The various data on geometrical parameters included in Fig. 4 all reveal the same conclusions regarding the convergence. Smaller basis sets like I and II are clearly inadequate for a reliable reproduction of the optimized geometry. Some geometrical parameters are even strongly deviating from the convergence values. Regardless of the choice of the functional form, the geometrical parameters converge from basis set III onwards.

The largest relaxations are observed for the alkali ions and in particular those located in the *xz*-plane (Na(1) ions in Fig. 4b and 4c. The relaxations of the halide ions on the other hand are rather small. Only the halide ions in line with the S_2^- defect axis ([110] direction) are subject to somewhat larger relaxations.

As a general protocol, we propose basis set IV for further calculations in this paper for geometry optimizations in ADF because this basis set gives an excellent compromise between computation time and numerical accuracy.

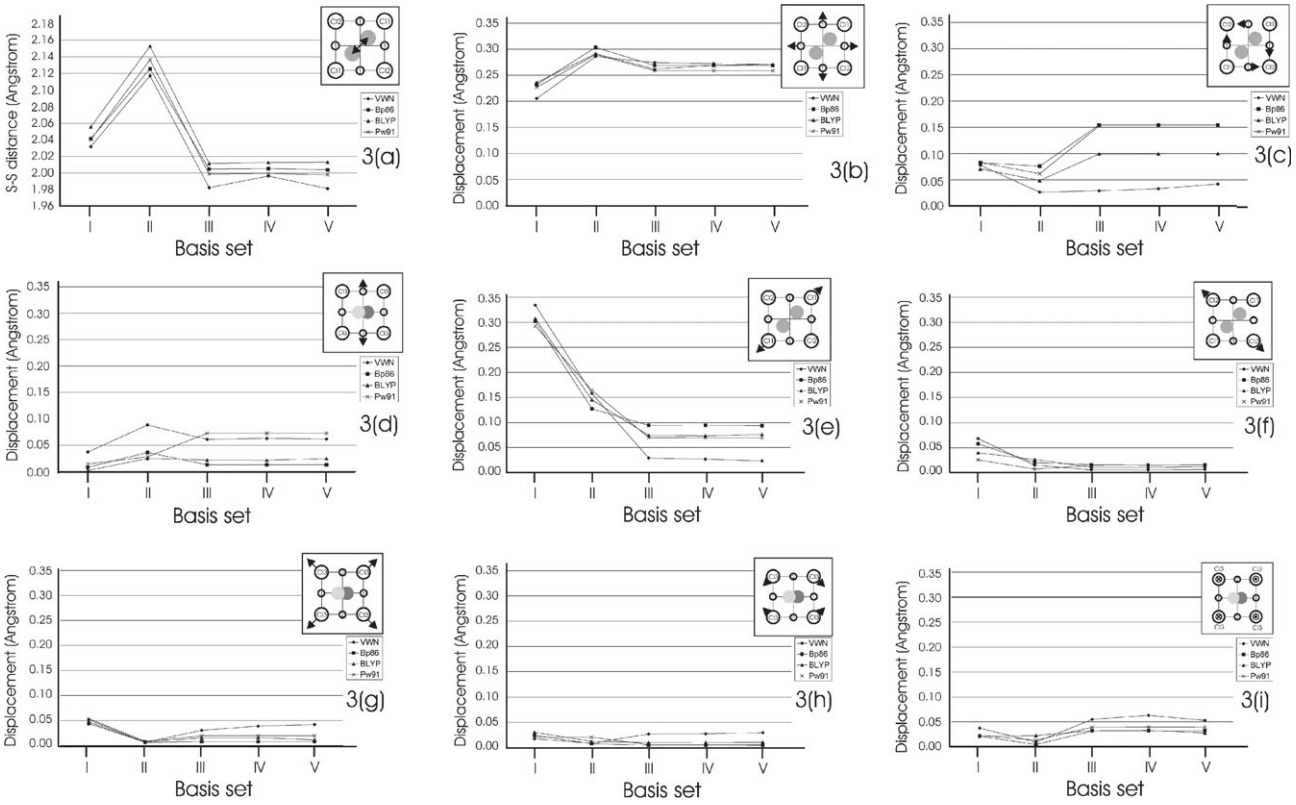

Fig. 4 Relaxations of the first two lattice shells for the NaCl: S_2^- defect structure as a function of increasing basis set. The internuclear distance of the S_2^- molecular ion is shown in (a). The directions and magnitudes of the relaxations for the first lattice shell of alkali ions are shown in (b), (c) and (d). The relaxations of the ions of the second lattice shell: Cl1, Cl2 and Cl3 are shown in (e), (f), (g), (h) and (i).

The data in Fig. 4 also reveal additional information on the impact of the functional on the geometry. They all show similar convergence features, as already mentioned, but apart from some specific relaxations (Fig. 4c, 4d and 4e) all other predicted geometrical parameters are of the same magnitude.

Influence of geometry on theoretical EPR values. Accurate geometries have been identified as an important factor in the calculation of EPR tensors of main group radicals and transition metal complexes.[88] For the systems under study, no direct experimental geometry data are available and thus the only way to examine the ''quality'' of the geometry is based on a comparative study of derived quantities as *e.g.* *g*-values. It is important to examine the sensitivity of these results to changes in the geometrical parameters.

Fig. 5 displays the theoretical *g*-values for the S_2^- defect in NaCl. The figure is organized as follows. We distinguish five clusters. Each cluster belongs to a specific level of theory for the evaluation of the *g*-values. In each cluster four levels of theory are used for the geometry optimization: VWN/IV, Bp86/IV, BLYP/IV and Pw91/IV. The results in Fig. 5 reveal unambiguously a rather limited role of the geometry on the computed *g*-values, provided that at least a moderate basis set (like a double-ζ) is used in the geometry optimization. The largest fluctuations are noticed among the different clusters, emphasizing the importance of the functional used for the evaluation of *g*-parameters. This will be discussed in detail in the next subsection.

In summary, the functional form used during the geometry optimization has only a minor influence on the prediction of the *g*-values. In the general protocol, we use geometry optimizations within the VWN/IV level of theory throughout, because it offers a good compromise between accuracy and calculation time.

4.4. Level of theory dependence of the EPR parameters

We performed a complete set of calculations on diverse XY^- molecular ions in a variety of alkali halide lattices. The results are collected in S. Table II. The only common level of theory used is VWN/IV for the geometry optimization, as suggested by the protocol discussed in the preceding subsection.

The study of the level of theory (basis set and exchange correlation functional) and its influence on the predicted *g*-values is made as complete as possible. Because relatively few experimental hyperfine data are available, we shall focus on the *g*-values. The basis sets applied for describing the atomic orbitals of the defect do not necessarily coincide with those of the remaining lattice atoms. Experimental *g*-values are available for all considered defect structures, allowing a thorough validation of the protocol, which is the principal aim of this study. The main focus lies in the reproduction of the *g*-values, and in particular, in the reproduction of trends in the deviations from the free electron value when varying the defect or when changing the lattice environment. Absolute values for the g tensor and relative errors ($RE = 100(g_{exp} - g_{th})/g_{exp}$) are taken up in S. Table II, together with the deviation of g_z from the free electron value. The high number of calculations accomplished justifies the conclusions which will be made concerning the influence of basis sets and exchange correlation form on calculated *g*-values. The deviation of the g_z value from the free electron value is additionally plotted in Fig. 6 for various $MZ{:}XY^-$ defect structures and various functional forms.

Influence of basis sets. Within the same class of functional, multiple calculations have been performed with different basis sets for the defect and for the alkali and halide ions of the lattice. This investigation has been performed for all defects in the NaCl lattice (S. Table II). The influence on the *g*-values is not overwhelming. On the contrary, only little fluctuations are noticed. In the literature, similar observations have been reported by Patchkovskii *et al.*[88] and Stein *et al.*[89]

The hybrid functionals have a common feature in predicting systematically *g*-values which are too close to the free electron value. For this class of functionals, the increasing deviation from the free electron value of g_z when increasing the size of the central molecular ion for a particular lattice environment is not reproduced theoretically. Enlargement of the basis set does not change this pattern in any sense. Basis set effects seem to be

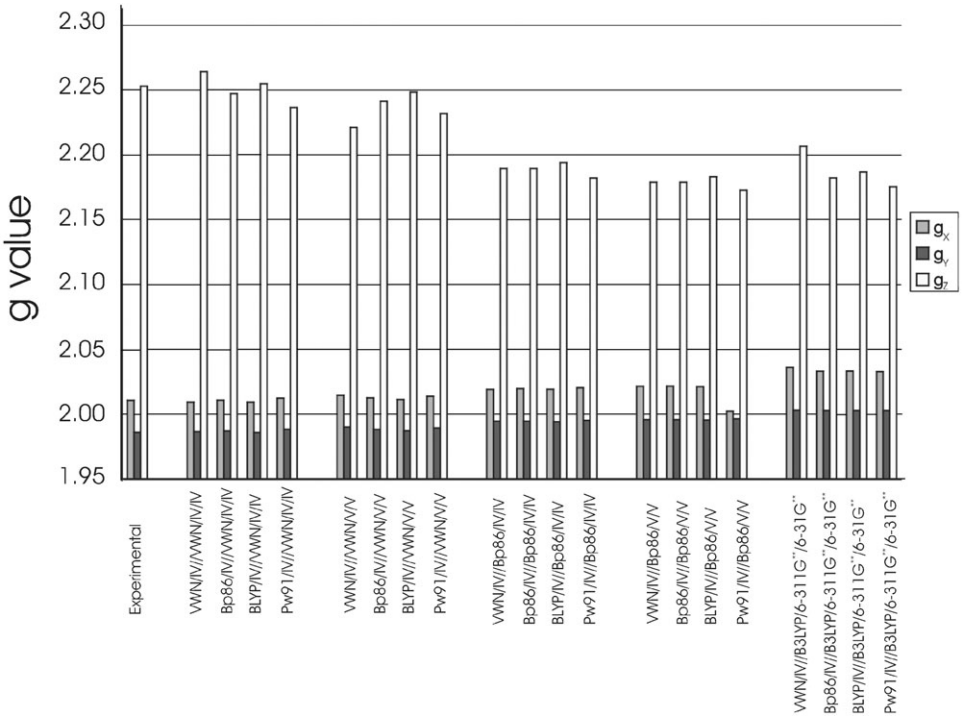

Fig. 5 Influence of the geometry on theoretical *g*-values for the NaCl: S_2^- defect structure. EPR calculations were performed using various levels of theory on geometries optimized with a VWN, Bp86, Pw91 or BLYP functional form and the basis set IV.

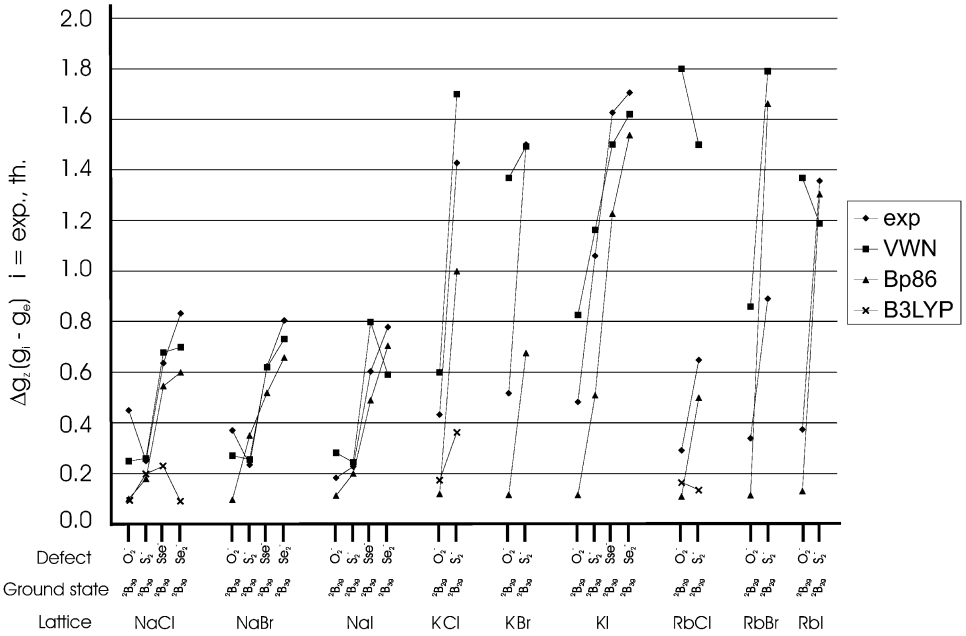

Fig. 6 Graphical representation of the data listed in S. Table II. For a particular functional form describing a certain defect structure, the main deviation from the free electron value is considered for g_z. For all defect structures, the ground state is listed.

more pronounced for the heavier RbZ lattices, but only in those classes of lattices the deviation from experiment is unacceptably high. Although the agreement with experiment improves, the final theoretical estimates still largely deviate from the experimental data. Indeed, for the RbCl : S_2^- defect structure, the relative error decreases from about 30% to 20% by adding polarization functions (using the VWN functional form) but the final value remains too far from experiment. For alkali halide lattices with smaller alkali atoms, the inclusion of polarization functions does not improve the agreement between experimental and predicted *g*-values. This is supported by the multiple theoretical data on the NaCl : S_2^- and KCl : S_2^- defect structures using the VWN functional form as implemented in G03.

Summarizing, triple-ζ basis sets are plausible for the description of small lattices like NaZ and KZ. This corresponds with basis set IV in ADF. Using G03, a 6-31G** and 6-311G** basis set for the lattice environment and the central molecular ion are suggested, respectively. For the heavier RbZ lattices, a triple-ζ basis set extended with additional polarization functions are recommended. In any case, basis set enlargement, when starting from a relatively accurate basis set (*i.e.* IV or 6-31G) will not drastically improve the agreement with experimental data.

Influence of the exchange correlation form. The main goal of this level of theory study is the search for a suitable functional which is able to give reliable predictions for the *g*-tensors of the XY^- defects doped in alkali halides and in particular reproduce the correct behavior of the deviations from the free electron value between various defects in the same lattice. The sensitivity of the *g*-values to the choice of the functional used for calculating them has already been stressed when discussing Fig. 5. Although the influence of basis set effects is rather limited, substantial fluctuations in theoretical *g*-values are found when different exchange correlation forms are used. Apparently, the best agreement with experimental data is found when using the VWN functional, for the S_2^- defect in the NaCl lattice (*cfr.* Fig. 5). The question arises to what extent these findings hold for other defects and/or other lattices. Concerning lattices with light alkali atoms, the predicted deviations from experiment are within the range of 10%, using VWN. But as soon we examine the results in RbZ lattices, the deviations increase dramatically. This forces us to analyze the theoretical results with another focus.

In Fig. 6 we display the behavior of the deviation of g_z from the free electron g value in function of the defect in each MZ lattice. In the three NaZ lattices taken into consideration, both LDA(VWN) and GGA(Bp86) functionals predict the correct trends in Δg_z, *i.e.* larger deviations from the free electron value are observed when the defect size increases. But once Rb atoms are considered, the VWN functional fails completely. On the other hand, the Bp86 functional succeeds in predicting the correct behavior and even the absolute values of g_z have an acceptable accuracy. We emphasize that the hybrid B3LYP functional fails in its totality and can therefore be rejected.

As is clear from the previous results, the calculated *g*-values are highly affected by the exchange correlation form. The choice of the basis set used for constructing the EPR parameters as well as the used geometry have only a minor influence. For small lattices, the VWN and Bp86 functional show comparable accuracy, while for the heavier lattices, it turns out that the Bp86 functional is superior to VWN. The B3LYP functional fails completely. As has been mentioned above, the computed *g*-values are highly affected by covalency effects. As is well known in literature,[90–93] hybrid functionals tend to overestimate covalency effects, leading to *g*-shifts too close to the free electron value. Consequently, the origin of the less agreement between experimental and computed *g*-values using hybrid functionals, lies in the improper description of covalency effects, while the used basis set or geometrical structure has only a minor influence. In the search for an ''ideal'' functional meeting the following basic criteria: (i) correct reproduction of trends in experimental *g*-values when increasing the defect size or lattice environment and (ii) accurate prediction of the deviations from the free electron value, we can state that the Bp86 exchange correlation form gives an overall satisfactory description for the whole variety of MZ : XY^- defect structures. Nevertheless, for the smaller lattices, the Bp86 functional form gives a good qualitative picture while the VWN functional form gives slightly better quantitative agreement.

As is clear from Fig. 6 for the computed $^2B_{2g}$ ground state results, a systematic overestimation of the experimental Δg_z values occurs when using the LDA and a underestimation when using GGA and hybrid functional forms. Similar

remarks have been made in many applications of density functional methods to EPR and nuclear magnetic resonance properties of main group compounds or main group nuclei in transition metal complexes.[90–93] This systematic deviation from the experimental Δg values is related to an improper description of covalency effects. As has been shown by Känzig *et al.*,[7] covalency effects give negative contributions to the *g*-shift. Thus, when the overlap between the paramagnetic lobes which contain the unpaired electron and the ions which make up the lattice environment is predicted to be too large (small) in the DFT calculation, the theoretical *g*-shifts become too small (large) accordingly. These observations are consistent with the idea that the GGA and hybrid functionals tend to overestimate covalency effects.[94–99]

For completeness, theoretical hyperfine values were compared with the available experimental data. These data are given in Table III of the ESI.† In Table IV, theoretical hyperfine values are compared with the available experimental ones for all MZ: XY^- defect structures. The results are not in conflict with the above conclusions.

Finally, we find an interesting feature in comparing ADF and G03 results for the *g*-values when using the same functional. Although the use of different basis sets (Slater type orbitals and Gaussian type orbitals, respectively) hinders a direct comparison, we notice large similarities in the patterns. The same conclusions were made in the work of Saladino *et al.*[100]

Reproduction of the correct ground state of the defect. The whole analysis up to now and the recommendation of the GGA functional in the protocol for the evaluation of the *g*-values are based on the reproduction of the g_z value, being the g component along the internuclear axis of the diatomic defect. It is well known that a strong correlation exists between the g_z value and the two components perpendicular to the z axis.[7–9]. Large deviations of g_z from the free electron value systematically generate large deviations of g_x and g_y from the free electron value too. *In vacuo*, the *g*-values for the XY^- defect have the extreme values: $g_z = 4$ and $g_x = g_y = 0$ since the paramagnetic lobes of the unpaired electron are undetermined in the *xy*-plane. Due to the crystal environment, the degeneracy of the spatial orientation of the p-lobe is lifted and the [001] and [$\bar{1}$10] crystal axes arise as preferred directions in a natural way. The ultimate orientation of the paramagnetic lobes which contain the unpaired electron in the ground state configuration, is a subtle combination of diverse factors. In this single-vacancy model the unpaired electron of the central XY^- defect is submitted to (i) the electrostatic interaction with the whole cluster (composed of 88 atoms in this work) and (ii) the covalent interactions with the nearest lattice atoms. The delicate interplay of these interactions excludes a straightforward determination of the ground state, based on geometrical grounds. We are only able to state some loose conclusions. If the defect is small in comparison with the halide ion it replaces, there is a tendency for a $^2B_{2g}$ ground state (Fig. 1a) with the paramagnetic lobes in the *xz*-plane. This results in a g_x value smaller than g_y. If the size of the central molecular ion increases with respect to the volume of the halide vacancy, the paramagnetic lobes of the unpaired electron tend rather to be oriented toward the nearest alkali atoms along the *y* axis (Fig. 1b), leading to a $^2B_{3g}$ ground state.

In this $^2B_{3g}$ ground state, small covalent interactions are observed with eight large halide ions located on a (110) position. Due to these small covalent interactions, both LDA and GGA give similar accuracy. The situation is totally different for defects in the $^2B_{2g}$ ground state. For this ground state, large covalent interactions with the nearest four alkali ions located in the *xz*-plane occur. The correct reproduction of the *g*-values for the $^2B_{2g}$ ground state defects is apparently more sensitive to local parameters and the choice of the functional. Due to an underestimation of these covalent effects, the VWN functional form fails completely in these cases, while the Bp86 functional form gives a better description of these covalent effects.

For both ground state defects, the Bp86 functional fulfils the criteria imposed for an ideal functional form as stated in the previous section. Finally, we stress the ability of each functional to predict the correct ground state of the defect as can be seen from Table II of the ESI.†

4.5. Flow scheme

In the previous sections, a computational protocol for simulating *g*-tensors of chalcogen defects in alkali halide lattices was derived and applied to the XY^- defects located in a single-vacancy configuration. In this section, the recommended flow scheme is summarized.

• **Cluster size.** Clusters with a low total charge and an accurate electrostatic Madelung potential at the defect site are preferred: for simulating the single-vacancy model, a cluster size of 88 atoms is found to be sufficient and feasible in ADF.

• **Lattice relaxation.** The number of relaxed lattice shells around the central defect is determined by obtaining convergence of the theoretical *g*-values as a function of relaxed lattice shells: in this work, the central molecular ion (the XY^- defect) and at least the nearest two lattice shells should be relaxed.

• **Level of theory for the optimization.** Here, convergence of the relaxation of the lattice environment as a function of increasing basis set for various functional forms is to be investigated: for the MZ : XY^- defect structures, the geometry optimization might be performed within the following levels of theory: (1) basis set IV and (2) use of the VWN functional as implemented in the ADF package.

• **Level of theory for the EPR calculation.** Finally, the influence of basis set effects and exchange correlation functional on the theoretical EPR data has to be investigated. (i) Choice of basis set: basis sets of sufficient quality, like a triple-ζ, are recommended for the simulation of the NaZ and KZ lattices, while polarization functions have an important influence for the RbZ lattices. (ii) Choice of exchange correlation form: both the VWN and Bp86 functional form are suitable to describe the XY^- defects located in a single-vacancy configuration for the NaZ and KZ lattices. For the heavier RbZ lattices, or defects in a $^2B_{2g}$ ground state, only the Bp86 exchange correlation fulfils the required criteria.

5. Conclusion

A thorough level of theory study has been performed with the principal goal of constructing a reliable protocol for the description of the *g*-tensors of chalcogen doped alkali halide lattices. The study was based on diatomic chalcogen defects located in a single-vacancy configuration. A flow scheme is presented which can be applied to other chalcogen ions in these lattices. The principal conclusions for XY^- defects in MZ lattices are:

(i) the limitation to 88 atoms for an accurate description of the lattice environment.

(ii) the Bp86 exchange correlation functional as the most suitable functional for an overall agreement.

(iii) the necessity of using large basis sets like IV and V as implemented in the ADF program package.

(iv) the complete failure of the hybrid functionals for predicting correct *g*-parameters.

The protocol was mainly derived for *g*-values and it may not give the same accuracy for hyperfine values. Because few

experimental hyperfine values are available, no final statement concerning these data can be made.

Acknowledgements

Fruitful discussions with D. Van Neck are gratefully acknowledged. The authors would like to thank the Fund for Scientific Research (FWO-Flanders, Belgium) and the Research board of Ghent University for financial support. V. Van Speybroeck and H. Vrielinck thank the Fund for Scientific Research—Flanders for a postdoctoral fellowship.

References

1 M. Ashida, O. Morikawa, H. Arai and R. Kato, *Prog. Cryst. Growth Charact. Mater.*, 1996, **33**(1–3), 105.
2 R. Ye, H. Tazawa, M. Baba, K. Nishidate, L. O. Schwan and D. Schmid, *Jpn. J. Appl. Phys. Part 2*, 1998, **37**, L1154.
3 R. Ye, H. Tazawa, M. Baba, K. Nishidate, L. O. Schwan and D. Schmid, *J. Lumin.*, 2000, **87**, 542.
4 A. A. Kalachev and V. V. Samartsev, *Laser Phys.*, 2002, **12**(8), 1114.
5 M. A. J. Rodgers and E. L. Poweres, *Oxyradicals in Chemistry and Biology*, Academic Press, New York, 1981.
6 I. Fridovich I, *J. Biol. Chem.*, 1997, **272**(30), 18515.
7 W. Känzig and M. H. Cohen, *Phys. Rev. Lett.*, 1959, **3**, 509.
8 R. Zeller and W. Känzig, *Helv. Phys. Acta*, 1967, **40**, 845.
9 R. T. Shuey and H. R. Zeller, *Helv. Phys. Acta*, 1967, **40**, 873.
10 J. R. Morton, *J. Chem. Phys.*, 1965, **43**, 3418.
11 J. R. Morton, *J. Phys. Chem.*, 1967, **71**, 89.
12 L. E. Vannotti and J. R. Morton, *Phys. Rev.*, 1967, **161**, 282.
13 L. E. Vannotti and J. R. Morton, *Phys. Lett. A*, 1967, **24**, 250.
14 F. Callens, P. Matthys and E. Boesman, *Phys. Status Solidi B*, 1983, **118**(1), K35.
15 P. Matthys, F. Callens and E. Boesman, *Solid State Commun.*, 1983, **45**(1), 1.
16 F. Callens, F. Maes, P. Matthys and E. Boesman, *J. Phys. Condens. Matter*, 1989, **1**(1), 6921.
17 F. Maes, F. Callens, P. Matthys and E. Boesman, *J. Phys. Chem. Solids*, 1990, **51**(11), 1289.
18 F. Maes, F. Callens, P. Matthys and E. Boesman, *Phys. Status Solidi B*, 1990, **161**(1), K1.
19 F. Maes, P. Matthys, F. Callens and E. Boesman, *Solid State Commun.*, 1991, **80**(8), 583.
20 F. Maes, P. Matthys, F. Callens, P. Moens and E. Boesman, *J. Phys., Condens. Matter*, 1992, **4**(1), 249.
21 F. Maes, S. Van Doorslaer, F. Callens, P. Moens, P. Matthys and E. Boesman, *J. Phys.: Condens. Matter*, 1994, **6**(39), 8065.
22 S. Van Doorslaer, F. Maes, F. Callens, P. Moens and E. Boesman, *J. Chem. Soc., Faraday Trans.*, 1994, **90**(17), 2541.
23 S. Van Doorslaer, F. Callens, F. Maes and P. Matthys, *J. Phys., Condens. Matter*, 1995, **7**(48), 9279.
24 S. Van Doorslaer, F. Callens, F. Maes and E. Boesman, *Phys. Rev. B*, 1996, **54**(2), 1145.
25 S. Van Doorslaer, F. Maes F. Callens, P. Matthys and E. Boesman, *J. Chem. Soc., Faraday Trans.*, 1996, **92**(9), 1579.
26 F. Stevens, H. Vrielinck, F. Callens, E. Pauwels and M. Waroquier, *Phys. Rev. B*, 2002, **66**, 134103.
27 F. Stevens, H. Vrielinck, F. Callens, E. Pauwels and M. Waroquier, *Phys. Rev. B*, 2003, **67**, 104429.
28 A. A. Leitão, N. V. Vugman and C. E. Bielschowski, *Chem. Phys. Lett.*, 2000, **321**, 269.
29 A. A. Leitão, J. A. C. Neto, N. M. Pinhal, C. E. Bielschowsky and N. V. Vugman, *J. Phys. Chem. A*, 2001, **105**(3), 614.
30 A. A. Leitão, N. V. Vugman and C. E. Bielschowsky, *J. Phys. Chem. A*, 2002, **106**(41), 9569.
31 A. A. Leitão, R. B. Capaz, N. V. Vugman and C. E. Bielsehowsky, *J. Mol. Struc.-Theochem.*, 2002, **580**, 65.
32 P. Garcia-Fernandez, J. A. Aramburu, M. T. Barriuso and M. Moreno, *Radiat. Eff. Defects Solids*, 2002, **157**(6–12), 829.
33 M. T. Barriuso, J. A. Aramburu and M. Moreno, *J. Phys.: Condens. Matter*, 2002, **14**(25), 6521.
34 M. T. Barriuso, P. G. Fernandez, J. A. Aramburu and M. Moreno, *Radiat. Eff. Defects Solids*, 2003, **158**(1–6), 131.
35 N. M. Atherton, *Principles of Electron Spin Resonance*, Prentice Hall, New York, 1993.
36 *ADF*, http://tc.chem.vu.nl/SCM, Department of Theoretical Chemistry, Vrije Universiteit Amsterdam.
37 E. J. Baerends, D. E. Ellis and P. Ros, *Chem. Phys.*, 1973, **2**, 41.
38 F. Guerra, O. Visser, J. G. Snijders, G. ter Velde and E. J. Baerends, in *Methods and Techniques in Computational Chemistry METECC-95*, eds. E. Clementi and G. Corongiu, Cagliari, 1995, pp. 305-395.
39 S. H. Vosko, L. Wilk and M. Nusair, *Can. J. Phys.*, 1980, **58**(8), 1200.
40 J. P. Perdew, *Phys. Rev. B*, 1986, **33**(12), 8822.
41 A. D. Becke, *Phys. Rev. A*, 1988, **38**(6), 3098.
42 C. Lee, W. Yang and R. G. Parr, *Phys. Rev. B*, 1988, **37**, 785.
43 B. C. Johnson, P. M. W. Gill and J. A. Pople, *J. Chem. Phys.*, 1993, **98**(7), 5612.
44 T. V. Russo, R. L. Martin and P. J. Hay, *J. Chem. Phys.*, 1994, **101**(9), 7729.
45 J. P. Perdew, J. A. Chevary, S. H. Vosko, K. A. Jackson, M. R. Pederson, D. J. Singh and C. Fiolhais, *Phys. Rev. B*, 1992, **46**(11), 6671.
46 E. van Lenthe, P. Wormer and A. van der Avoird, *J. Chem. Phys.*, 1997, **107**(7), 2488.
47 E. van Lenthe, A. van der Avoird and P. Wormer, *J. Chem. Phys.*, 1997, **108**(12), 4783.
48 F. Herman and F. Skilman, *Atomic Structure Calculations*, Prentice-Hall, Engelwood Cliffs, NJ, 1963.
49 M. J. Frisch, G. W. Trucks, H. B. Schlegel, G. E. Scuseria, M. A. Robb, J. R. Cheeseman, J. A. Montgomery Jr., T. Vreven, K. N. Kudin, J. C. Burant, J. M. Millam, S. S. Iyengar, J. Tomasi, V. Barone, B. Mennucci, M. Cossi, G. Scalmani, N. Rega, G. A. Petersson, H. Nakatsuji, M. Hada, M. Ehara, K. Toyota, R. Fukuda, J. Hasegawa, M. Ishida, T. Nakajima, Y. Honda, O. Kitao, H. Nakai, M. Klene, X. Li, J. E. Knox, H. P. Hratchian, J. B. Cross, C. Adamo, J. Jaramillo, R. Gomperts, R. E. Stratmann, O. Yazyev, A. J. Austin, R. Cammi, C. Pomelli, J. W. Ochterski, P. Y. Ayala, K. Morokuma, G. A. Voth, P. Salvador, J. J. Dannenberg, V. G. Zakrzewski, S. Dapprich, A. D. Daniels, M. C. Strain, O. Farkas, D. K. Malick, A. D. Rabuck, K. Raghavachari, J. B. Foresman, J. V. Ortiz, Q. Cui, A. G. Baboul, S. Clifford, J. Cioslowski, B. B. Stefanov, G. Liu, A. Liashenko, P. Piskorz, I. Komaromi, R. L. Martin, D. J. Fox, T. Keith, M. A. Al-Laham, C. Y. Peng, A. Nanayakkara, M. Challacombe, P. M. W. Gill, B. Johnson, W. Chen, M. W. Wong, C. Gonzalez and J. A. Pople, *GAUSSIAN 03, (Revision A.1)*, Gaussian, Inc., Pittsburgh PA, 2003.
50 A. D. Becke, *J. Chem. Phys.*, 1993, **98**, 5648.
51 J. P. Perdew, J. A. Chevary, S. H. Vosko, K. A. Jackson, M. R. Pederson, D. J. Singh and C. Fiolhais, *Phys. Rev. B*, 1993, **48**(7), 4978.
52 J. P. Perdew, K. Burke and Y. Wang, *Phys. Rev. B*, 1996, **54**(23), 16533.
53 J. P. Perdew, K. Burke and M. Ernzerhof, *Phys. Rev. Lett.*, 1997, **78**(7), 1396.
54 A. Frisch, M. J. Frisch and G. W. Trucks, *GAUSSIAN 03 Users Reference*, Gaussian Inc., 2003.
55 Basis sets were obtained from the Extensible Computational Chemistry Environment Basis Set Database, Version 6/19/03, as developed and distributed by the Molecular Science Computing Facility, Environmental and Molecular Sciences Laboratory-which is part of the Pacific Northwest Laboratory, P.O. Box 999, Richland, Washington 99352, USA, and funded by the US Department of Energy. The Pacific Northwest Laboratory is a multi-program laboratory operated by Battelle Memorial Institute for the US Department of Energy under contract DE-AC06-76RLO 1830. Contact David Feller or Karen Schuchardt for further information.
56 E. Glendening, D. Feller and M. Thompson, *J. Am. Chem. Soc.*, 1994, **116**, 10657.
57 V. Barone, in *Recent Advances in Density Functional Methods*, ed. D. P. Chong, World Scientific, Singapore, 1996.
58 P. C. Hariharan and J. A. Pople, *Theor. Chim. Acta*, 1973, **28**, 213.
59 M. M. Francl, W. J. Petro, W. J. Hehre, J. S. Binkley, M. S. Gordon, D. J. DeFrees and J. A. Pople, *J. Chem. Phys.*, 1982, **77**, 3654.
60 J. A. Pople, *J. Chem. Phys.*, 1980, **72**, 650.
61 J.-P. Blaudeau, M. P. McGrath, L. A. Curtiss and L. Radom, *J. Chem. Phys.*, 1997, **107**, 5016.
62 L. A. Curtiss, M. P. McGrath, J.-P. Blaudeau, N. E. Davis, R. C. Binning and L. Radom, *J. Chem. Phys.*, 1995, **103**, 6104.
63 T. H. Dunning, *J. Chem. Phys.*, 1989, **90**, 1007.
64 D. E. Woon and T. H. Dunning, *J. Chem. Phys.*, 1993, **98**, 1358.
65 K. A. Peterson and T. H. Dunning, *J. Chem. Phys.*, 2002, **117**, 10548.

66 A. J. Sadlej, *Collect. Czech. Chem. Commun.*, 1988, **53**, 1995.
67 A. J. Sadlej, *Theor. Chim. Acta*, 1992, **79**, 123.
68 A. J. Sadlej, *Theor. Chim. Acta*, 1992, **81**, 45.
69 A. J. Sadlej, *Theor. Chim. Acta*, 1992, **81**, 339.
70 F. Neese, *J. Chem. Phys.*, 2001, **115**, 11080.
71 J. E. Harriman, *Theoretical Foundations of Electron Spin Resonance*, Academic Press, New York, 1978.
72 C. Chang, M. Pelissier and P. Durand, *Phys. Scr.*, 1986, **34**, 394.
73 J.-L. Huelly, I. Lindgren, E. Lindroth, S. Lundqvist and A. M. Martensson-Pendrill, *J. Phys. B*, 1986, **19**, 2799.
74 E. Van Lenthe, E. J. Baerends and J. Snijders, *J. Chem. Phys.*, 1993, **99**, 4597.
75 E. Pauwels, V. Van Speybroeck, P. Lahorte and M. Waroquier, *J. Phys. Chem. A*, 2001, **105**, 8794.
76 N. Papanikolaou, R. Zeller, P. H. Dederichs and N. Stefanou, *Comput. Mater. Sci.*, 1997, **8**(1–2), 131.
77 C. P. Ewels, R. Jones, S. Oberg, J. Miro and P. Deak, *Phys. Rev. Lett.*, 1996, **77**(5), 865.
78 K. Jackson, M. R. Pederson and B. M. Klein, *Phys. Rev. B*, 1991, **43**(3), 2364.
79 F. Stevens, H. Vrielinck, F. Callens and M. Waroquier, *Solid State Commun.*, 2004, **132**(11), 787.
80 H. M. Evjen, *Phys. Rev.*, 1932, **39**, 675.
81 N. W. Winter, R. M. Pitzer and D. K. Temple, *J. Chem. Phys.*, 1987, **86**, 3549.
82 N. W. Winter, R. M. Pitzer and D. K. Temple, *J. Chem. Phys.*, 1987, **87**, 2945.
83 S. Brazzelli, C. Di Valentin, G. Pacchioni, E. Giamello and M. Chiesa, *J. Phys. Chem. B*, 2003, **107**, 8498.
84 R. Car and M. Parrinello, *Phys. Rev. Lett.*, 1985, **55**, 2471.
85 V. Van Speybroeck, E. Pauwels, F. Stevens, F. Callens and M. Waroquier, *Int. J. Quantum Chem.*, 2004, accepted.
86 J. Hutter, P. Ballone, M. Bernasconi, P. Focher, E. Fois, S. Goedecker, M. Parrinello and M. E. Tuckermann, *CPMD V3.7*, Copyright IBM Corp 1990–2003, Copyright MPI für Festkörperforschung Stuttgart, 1997–2001.
87 R. E. Crandall, *Exp. Math.*, 1999, **8**(4), 367.
88 S. Patchkovskii and T. Ziegler, *J. Chem. Phys.*, 1999, **111**(13), 5730.
89 M. Stein, E. van Lenthe, E. J. Baerends and W. Lubitz, *J. Phys. Chem. A*, 2001, **105**(2), 416.
90 V. G. Malkin, O. L. Malkina, M. E. Casida and D. R. Salahub, *J. Am. Chem. Soc.*, 1994, **116**(13), 5898.
91 L. Olsson and D. Cremer, *J. Chem. Phys.*, 1996, **105**, 8995.
92 P. Belanzoni, E. J. Baerends and M. Gribnau, *J. Phys. Chem. A*, 1999, **103**(19), 3732.
93 M. Kaupp, C. Remenyi, J. Vaara, O. L. Malkina and V. G. Malkin, *J. Am. Chem. Soc.*, 2002, **124**(11), 2709.
94 K. W. Penfield, A. A. Gewirth and E. I. Solomon, *J. Am. Chem. Soc.*, 1985, **107**(15), 4519.
95 J. Swann and T. D. Westmoreland, *Inorg. Chem.*, 1997, **36**(23), 5348.
96 M. Munzarova and M. Kaupp, *J. Phys. Chem. A*, 1999, **103**(48), 9966.
97 G. Schreckenbach, *J. Chem. Phys.*, 1999, **110**(24), 11936.
98 F. Neese, *J. Phys. Chem. A*, 2001, **105**, 4290.
99 A. V. Arbuznikov, M. Kaupp, V. G. Malkin, R. Reviakine and O. L. Malkina, *Phys. Chem. Chem. Phys.*, 2002, **4**(22), 5467.
100 A. C. Saladino and S. C. Larsen, *J. Phys. Chem. A*, 2003, **107**(11), 1872.